Absolute Quantitation of Cardiac ^{99m}Tc-Pyrophosphate Using Cadmium-Zinc-Telluride–Based SPECT/CT

Sharmila Dorbala[1–3], Mi-Ae Park[1], Sarah Cuddy[2,3], Vasvi Singh[2], Kyle Sullivan[1], Sirwoo Kim[1], Rodney H. Falk[3], Viviany R. Taqueti[1,2], Hicham Skali[2], Ron Blankstein[2], Camden Bay[1], Marie F. Kijewski[1], and Marcelo F. Di Carli[1,2]

[1]Division of Nuclear Medicine, Department of Radiology, Brigham and Women's Hospital, Boston, Massachusetts; [2]CV Imaging Program, Cardiovascular Division, Brigham and Women's Hospital, Boston, Massachusetts; and [3]CA Program, Division of Cardiology, Department of Medicine, Brigham and Women's Hospital, Boston, Massachusetts

The primary aims of this study were to determine the correlation between absolute quantitative ^{99m}Tc-pyrophosphate metrics and traditional measures of cardiac amyloid burden and to measure the intraobserver repeatability of the quantitative metrics. **Methods:** We studied 72 patients who underwent ^{99m}Tc-pyrophosphate SPECT/CT using a novel general-purpose cadmium-zinc-telluride–based SPECT/CT system. The clinical standard for these studies is visual grading (with grades of 0, 1, 2, and 3 indicating myocardial uptake absent, less than rib uptake, equal to rib uptake, or more than rib uptake, respectively). A visual grade of 2 or more was considered positive. For 72 patients, SUV_{max}, SUV_{mean}, cardiac amyloid activity (CAA; i.e., $SUV_{mean} \times$ left ventricular [LV] volume), and percentage injected dose (%ID) were calculated, and visual grading was performed. The correlation was determined between the 4 quantitative metrics or visual grades and the LV mass index (LVMI) (indexed to body surface area on echocardiography, 67 patients). For a subset of 11 patients, the correlation was determined between the visual or quantitative metrics and the extracellular volume (ECV) on cardiac MRI. Normal linear regression was used to compare the standardized association of each of the 4 quantitative metrics with LVMI, as a surrogate for amyloid burden. Receiver-operating-characteristic curve analysis was used to determine the diagnostic accuracy of quantitative metrics, using visual grading as the reference standard. The intraobserver repeatability of generating quantitative metrics was also determined. **Results:** All 4 quantitative metrics were highly accurate, with an area under the receiver-operating-characteristic curve of more than 0.96 for diagnosis of transthyretin cardiac amyloidosis. SUV_{max}, SUV_{mean}, CAA, %ID, and visual grade were moderately positively correlated with LVMI ($r = 0.485$ for %ID) and strongly positively correlated, albeit in a small cohort, with ECV ($r = 0.873$, SUV_{max}). Intraobserver repeatability was excellent, with less than a 2% coefficient of variation for SUV_{max}, %ID, and CAA and 3.8% for SUV_{mean}. All 4 quantitative metrics had a standardized effect of more than 0.324 on LVMI; the largest standardized effect was 0.485, for %ID. **Conclusion:** In this first (to our knowledge) study of ^{99m}Tc-pyrophosphate cardiac imaging using a novel cadmium-zinc-telluride SPECT/CT scanner, SUV_{max}, SUV_{mean}, CAA, and %ID measured by absolute quantitation of ^{99m}Tc-pyrophosphate were moderately correlated with LVMI and strongly correlated, albeit in a small cohort, with ECV. The intraobserver repeatability of generating the quantitative metrics was excellent.

Received Apr. 14, 2020; revision accepted Aug. 6, 2020.
For correspondence or reprints contact: Sharmila Dorbala, Brigham and Women's Hospital, 75 Francis St., Boston, MA 02115.
E-mail: sdorbala@bwh.harvard.edu
Published online Sep. 4, 2020.

Key Words: quantitative SPECT; ^{99m}Tc-pyrophosphate; pyrophosphate; CZT SPECT/CT

J Nucl Med 2021; 62:716–722
DOI: 10.2967/jnumed.120.247312

A highly specific tool that has emerged to non-invasively diagnose transthyretin (ATTR) cardiac amyloidosis (CA) is ^{99m}Tc-pyrophosphate (*1*). Relative ^{99m}Tc-pyrophosphate SPECT and planar imaging are the current standard for noninvasive diagnosis of ATTR CA. ^{99m}Tc-pyrophosphate SPECT is nearly 100% specific for ATTR in patients with heart failure and typical phenotypic features of amyloidosis on echocardiography or cardiac MRI (CMR) after exclusion of amyloid light-chain amyloidosis (*2*). However, current visual grading or semiquantitative approaches to interpretation (heart-to-contralateral ratio or heart–to–whole-body ratio), although adequate for diagnosis, are inadequate for detection of early disease, identification of response to therapy, and assessment of risk. Left ventricular (LV) mass by echocardiography and extracellular volume (ECV) by CMR are the current quantitative tools used to estimate cardiac amyloid burden and response to therapy. Newly developed SPECT technology with CT-based attenuation correction, cadmium-zinc-telluride (CZT)–based detection systems with high sensitivity, and a novel 360° geometry raise the possibility of enhanced quantitative SPECT (*3*).

The primary aims of this study were, first, to measure the correlation between ^{99m}Tc-pyrophosphate SPECT/CT absolute quantitative metrics, as well as visual grading, and both LV mass index (LVMI) and ECV and, second, to measure the intraobserver repeatability of the quantitative metrics.

MATERIALS AND METHODS

Study Cohort and Procedures

Consecutive patients over a 6-mo period with known or suspected CA referred clinically for ^{99m}Tc-pyrophosphate imaging and scanned using a general-purpose CZT SPECT/CT scanner (Veriton-CT; Spectrum Dynamics Inc) were included. Patients with systemic amyloid light-chain amyloidosis (by serum free-light-chain assay and serum and urine immunofixation electrophoreses) were excluded. TTR genetic testing was performed on all patients with positive ^{99m}Tc-pyrophosphate scan results. Most patients ($n = 67$) underwent a clinical echocardiogram (at a median of 5 d from the ^{99m}Tc-pyrophosphate scan), and a small subset of patients ($n = 11$; 5 patients with ATTR CA and 6 patients without ATTR CA by ^{99m}Tc-pyrophosphate scanning)

underwent a clinical CMR study (at a median of 61 d from the ^{99m}Tc-pyrophosphate scan). Clinical parameters, cardiac risk factors, clinical red flags for amyloidosis, and risk markers of serum estimated glomerular filtration rate and cardiac biomarker levels (N-terminal pro–B-type natriuretic peptide and high-sensitivity troponin-T) were obtained from medical records. The study was approved by the institutional Human Research Committee.

^{99m}Tc-Pyrophosphate SPECT/CT Methods

Acquisition. A 15-min chest SPECT/CT acquisition was performed 150–180 min after intravenous injection of 880.6 ± 66.6 MBq (23.8 ± 1.8 mCi) of ^{99m}Tc-pyrophosphate using a Veriton-CT imaging system. Attenuation correction was based on a low-dose unenhanced CT scan (effective exposure of 20 mAs, tube voltage of 120 kVP, free tidal breathing). Radiotracer dose and patient weight were recorded to produce quantitative SPECT images. ^{99m}Tc-pyrophosphate images were reconstructed onto a 256 × 256 matrix (2.46 × 2.46 × 2.46 mm voxel size) by ordered-subsets expectation maximization (4 iterations, 8 subsets), a gaussian filter of 4.48 mm in full width at half maximum, and a proprietary filter (interiteration convolution filter and postmedian filter) with corrections for radiotracer decay, point-spread function, scatter, and attenuation.

Qualitative ^{99m}Tc-Pyrophosphate Metrics. ^{99m}Tc-pyrophosphate SPECT images were reviewed by a single experienced physician observer who did not know the echocardiogram and CMR results and graded the images using a 0–3 scale (with grades of 0, 1, 2, and 3 indicating myocardial uptake absent, less than rib uptake, equal to rib uptake, or more than rib uptake, respectively). A visual grade of 2 or more on CZT SPECT/CT was considered positive for a final diagnosis of ATTR.

Quantitative ^{99m}Tc-Pyrophosphate Metrics. A volume of interest (VOI) was placed on the ^{99m}Tc-pyrophosphate images using the CT scan to define the external cardiac outline (Supplemental Fig. 1; supplemental materials are available at http://jnm.snmjournals.org). This VOI was edited on the fused ^{99m}Tc-pyrophosphate/CT images to include only LV uptake, as the right ventricular free-wall activity signal was often contaminated by sternal uptake. The VOI included the LV blood pool; we were not able to exclude the blood pool because CT contrast was not used, and early ^{99m}Tc-pyrophosphate blood-pool data were not acquired. This approach allowed us to quantify the visually negative cases. SUV (unitless) was defined as the decay-corrected activity concentration of ^{99m}Tc-pyrophosphate divided by injected activity per unit body weight. SUV_{max} and SUV_{mean} were the maximum and mean activity, respectively, within the VOI. The product of the VOI volume and SUV_{mean} defined integrated cardiac amyloid activity (CAA). Percentage injected dose (%ID) was defined as the absolute ^{99m}Tc-pyrophosphate activity concentration in the LV VOI multiplied by the VOI volume and divided by injected dose (decayed to scan start time). A single observer, masked to other results, derived these quantitative metrics using commercially available and validated software (MIM) (*4*); measurements were repeated after 2 wk by the same observer in a random sample of 14 studies to determine intraobserver repeatability.

CZT SPECT/CT System and Scanner Quality Control. The 360° CZT SPECT/CT device has 12 detector columns arranged in a circular ring with equal angular spacing. Each detector column has a 16 × 238 array of 2,048 pixelated CZT detectors, for a total of 24,576 CZT detectors in the system. Each detector has a size of 2.46 × 2.46 × 6 mm. Tungsten collimators are integrated with the CZT detectors, with a square hole size of 2.46 mm, septum thickness of 0.2 mm, and hole length of 24.5 mm. To ensure full-angular sampling of the patient body, each column swivels about its long axis and orbits counterclockwise about the central axis of the gantry.

The SPECT/CT system was calibrated for accurate quantitation using a uniform cylindric phantom filled with a known amount of ^{99m}Tc measured by a dose calibrator. The phantom data were reconstructed with ordered-subsets expectation maximization, including attenuation and scatter correction, and the cross-calibration factor between dose calibrator and SPECT images was then obtained to convert the voxel values in SPECT images into the absolute activity concentration, Bq/mL.

The stability of SPECT and CT is monitored daily using quality assurance testing before the first use on a patient. Energy resolution, detector uniformity, count sensitivity, center of rotation, and multiple-head registration of the SPECT system are quantitatively measured using a ^{57}Co rod source. For CT, the mean Hounsfield units of water and air, the SD of the water Hounsfield units, and artifacts are checked using a dedicated phantom.

Echocardiography Methods

Clinical standard 2-dimensional echocardiography was performed as per American Society of Echocardiography recommendations (*5*). Standard 2-dimensional measurements were made in triplicate; LV mass was derived using the Devereaux formula and was indexed to body surface area to derive LVMI.

CMR Methods

Contrast-enhanced CMR images were acquired on a 3.0-T system (Tim Trio; Siemens) as described previously (*6*). Briefly, the protocol consisted of steady-state free-precession cine imaging for assessing ventricular function and morphology, and native and postcontrast T1 mapping for quantification of myocardial ECV using a modified look-locker technique (with a 5-3-3 pattern). Segmental ECVs were calculated by the ratio of changes of relaxation rates of the myocardium to relaxation rates of blood and adjusted to the fractional blood volume of distribution (1 − hematocrit). Global myocardial ECV was then calculated by a single observer averaging the myocardial segmental ECVs from the short-axis slices at the base, mid, and apical LV levels. A commercial software package (MedisSuite, version 3.0; Medical Imaging Systems) was used to process and quantify the ECVs (*7*).

Statistics

Data are presented as mean ± SD or as medians with interquartile range, as appropriate, and compared using Student *t* tests and Wilcoxon rank-sum tests, respectively. Categoric variables were compared using Pearson χ^2 tests. An ANOVA with post hoc Bonferroni tests was used to compare quantitative ^{99m}Tc-pyrophosphate metrics by each category of visual grade. Pearson correlation analysis was used to determine the correlation between each of the 4 quantitative SPECT metrics with LVMI and ECV; Spearman correlation analysis was used for visual grading. Normal linear regression was used to determine the potential of the 4 quantitative metrics for prediction of LVMI. An attempt was made to use ridge regression to allow for the inclusion of all 4 highly correlated metrics in a single model. This was not successful, as one of the metrics maintained an unexpected association with LVMI unless a severe penalty was imposed. Therefore, 4 separate simple linear regression models were fit, and the magnitude of the standardized regression coefficients, as well as R^2, were compared among the 4 models. We standardized our predictors and response to allow comparison across models, as each quantitative metric is measured on a different scale. Receiver-operating-characteristic (ROC) curve analysis was used to determine the diagnostic accuracy of SUV_{max}, SUV_{mean}, CAA, and %ID, with visual grade–based classification as the reference standard. Unless otherwise stated, *P* values of less than 0.05 were considered statistically significant, and all testing was 2-tailed. Statistical analyses were performed using SPSS, version 20.0.0 (IBM Corp.).

RESULTS

The study cohort included 72 patients with known or suspected CA, 31.9% (23/72) of whom had positive ^{99m}Tc-pyrophosphate

scan results. The positive results were somewhat more often grade 3 (19.4%) than grade 2 (12.5%). Patients with ATTR CA ($n = 23$) were older, were nearly all male (22/23), experienced a greater frequency of musculoskeletal symptoms (Table 1), and manifested a distinct cardiac phenotype on echocardiography (Supplemental Table 1). None of these subjects had hereditary ATTR CA.

In 6 subjects we compared planar images from an NaI scanner with SPECT images from the CZT SPECT/CT scanner and found perfect concordance for normal–abnormal classification. Visual grade on planar NaI scans was 0 ($n = 2$) or 3 ($n = 2$) and was identical on CZT SPECT/CT scans. In 2 participants, visual grade was 1 on planar NaI SPECT scans and 0 on CZT/SPECT/CT scans (blood-pool activity).

We evaluated the distribution of the 4 novel quantitative metrics—SUV_{max}, SUV_{mean}, CAA, and %ID—for each of the 4 visual grading categories (Fig. 1 and Supplemental Fig. 2). These metrics, in general, tracked ^{99m}Tc-pyrophosphate visual grade, and intraobserver repeatability was excellent. Area under the ROC curve was more than 0.96 for each of the 4 quantitative metrics.

SUV_{max} and SUV_{mean}

Figure 2 shows the distribution of SUV_{max} for the 4 visual grades, its relationships to LVMI and to ECV, and its intraobserver repeatability. SUV_{max} was low and similar in grades 0 and 1 and high and similar in grades 2 and 3 (Fig. 2A). SUV_{max} was significantly lower in patients with grades 0 and 1 combined (no ATTR CA) than in those with grades 2 and 3 combined (ATTR CA, Table 2). Six patients with visual grades 0 and 1 had an SUV_{max} suggestive of disease presence (Fig. 2A). SUV_{max} was moderately positively correlated with LVMI (Fig. 2B) and strongly positively correlated with ECV (Fig. 2C). SUV_{max} was highly repeatable, with a coefficient of variation of 1.7%. SUV_{max} was strongly and positively correlated with visual grade ($r = 0.718$, $P < 0.0001$) and was highly accurate in diagnosing ATTR CA using visual grade as a reference (area under the ROC curve, 0.98; 95% CI, 0.959–1.0).

SUV_{mean} showed very similar findings (Supplemental Fig. 3; Table 2). Nine patients with visual grade 0 or 1 had an SUV_{max} suggestive of disease presence. SUV_{mean} was the least repeatable of the 4 metrics, with a coefficient of variation of 3.8%. SUV_{mean} was strongly and positively correlated with visual grade ($r = 0.732$, $P < 0.0001$) and was highly accurate in diagnosing ATTR CA using visual grade as a reference (0.97; 95% CI, 0.936–1.0).

CAA

Figure 3 shows the distribution of CAA for the 4 visual grades, its relationships to LVMI and to ECV, and its intraobserver repeatability. CAA was low and similar in patients with grade 0 or 1 and high and similar in those with grade 2 or 3 (Table 2). Five patients with visual grade 0 or 1 had CAAs that suggest disease presence (Fig. 3A). CAA was moderately and positively correlated with LVMI (Fig. 3B) and strongly and positively correlated with ECV (Fig. 3C). CAA was highly repeatable, with a coefficient of variation of 2.0%. CAA was strongly and positively correlated with visual grade ($r = 0.771$, $P < 0.0001$) and was highly accurate in diagnosing ATTR CA using visual grade as a reference (0.964; 95% CI, 0.927–1.0).

%ID

Figure 4 shows the distribution of %ID for the 4 visual grades, its relationships to LVMI and to ECV, and its intraobserver repeatability. %ID was low and similar in grades 0 and 1 and high and similar in grades 2 and 3 (Table 2). Four patients in visual grade 1 had %IDs that suggest disease presence (Fig. 4A). %ID was moderately and positively correlated with LVMI (Fig. 4B) and strongly and positively correlated with ECV (Fig. 4C). %ID was highly repeatable, with a coefficient of variation of 2.0%. %ID

TABLE 1
Baseline Characteristics

Characteristic	No ATTR CA ($n = 49$)	ATTR CA ($n = 23$)	*P*
Demographics			
Age (y)	73.7 ± 11.0	81.3 ± 8.1	0.004
Male	32 (65.3)	22 (95.7)	0.006
Body surface area (kg/m^2)	2.04 ± 0.29	1.95 ± 0.18	0.06
Risk factor history			
Hypertension	43 (89.6)	21 (91.3)	0.820
Hyperlipidemia	33 (70.2)	19 (82.6)	0.265
Heart failure	41 (83.7)	20 (87)	0.718
Coronary artery disease	18 (34.6)	11 (50)	0.324
Diabetes	20 (41.7)	10 (43.5)	0.885
Smoking	22 (45.8)	13 (56.5)	0.399
Pedal edema	26 (54.2)	10 (45.5)	0.498
Stroke	7 (14.6)	7 (30.4)	0.116
Musculoskeletal*	14 (30.4)	19 (82.6)	<0.0001
New York Heart Association class ≥ II	31 (64.5)	18 (78.3)	0.623

*Includes carpal tunnel syndrome, biceps tendon rupture, and lumbar spinal stenosis.
IQR = interquartile range.
Qualitative data are numbers followed by percentages in parentheses; continuous data are mean ± SD.

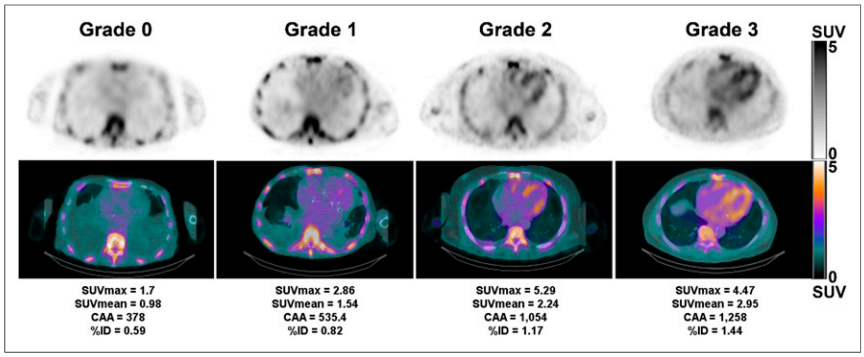

FIGURE 1. Representative ^{99m}Tc-pyrophosphate SPECT/CT images on SUV scale showing grades 0–3 uptake. Top row shows attenuation-corrected SPECT images, middle row shows SPECT/CT images, and bottom row shows corresponding SUV_{max}, SUV_{mean}, CAA, and %ID for each image.

was strongly and positively correlated with visual grade (r = 0.799, $P < 0.0001$) and was highly accurate in diagnosing ATTR CA using visual grade as a reference (area under the ROC curve, 0.97; 95% CI, 0.946–1.0).

Visual Grade

Visual grade was moderately and positively correlated with LVMI (r = 0.394, P = 0.001) and strongly and positively correlated with ECV (0.787, P = 0.004).

Predictors of LVMI

We performed normal linear regression analyses of each of the 4 quantitative metrics against LVMI (Table 3); ECV was not included because of the small sample size. We standardized our predictor and response to allow for comparison among metrics. Regression coefficients for all metrics were statistically significantly different from 0, with a P value of less than 0.001 for SUV_{max}, CAA, and %ID and a P value of 0.007 for SUV_{mean}. All R^2 values were greater than 0.104, with %ID having the highest, at 0.235. %ID had the highest standardized coefficient (0.485; 95% CI, 0.269–0.701).

DISCUSSION

We report several notable findings from this pilot study of quantitative ^{99m}Tc-pyrophosphate imaging using a novel general-purpose CZT scanner with 360° detector geometry. First, continuous quantitative measures of SUV_{max}, SUV_{mean}, CAA, and %ID were similarly low in patients with a visual grade of 0 or 1 and similarly high in those with a grade of 2 or 3. SUV_{max}, SUV_{mean}, %ID, and CAA, as well as visual grade, were moderately positively correlated with LVMI and strongly positively correlated, albeit in a small sample, with ECV. ^{99m}Tc-pyrophosphate visual grade correlated moderately with LVMI and strongly with ECV. Our sample size was not large enough to allow comparison of correlation coefficients among metrics, but the results suggest that SUV_{mean} was inferior to other quantitative metrics in terms of correlation with LVMI and intraobserver repeatability. This finding is not surprising, as SUV_{mean} is the metric that is most sensitive to VOI definition. Our results also suggest that %ID was stronger than the other 3 metrics in predicting amyloid burden by LVMI.

In this study, quantitative ^{99m}Tc-pyrophosphate measures were consistent with visual grade. Some patients in grades 0 and 1 had quantitative values similar to those of the patients diagnosed with ATTR CA, suggesting that quantitative SPECT has the potential to provide more granular information to diagnose amyloidosis than visual grade is able to provide. Our results align with, and add to, prior reports on ^{99m}Tc-DPD (^{99m}Tc-labeled 3,3-diphosphono-1,2-propanodicarboxylic acid) with the latest scanners in small cohorts (*8*), and using %ID and older-generation SPECT/CT scanners with ECV correlation in larger cohorts (*9*), showing similar quantitative measures between a visual grade of 0 or 1 and a visual grade of 2 or 3. Advances in SPECT instrumentation and software, notably CT-based attenuation correction, high-sensitivity 360° CZT-based scanners, and improved reconstruction algorithms, may further improve the accuracy of SPECT with absolute quantitation (*10*).

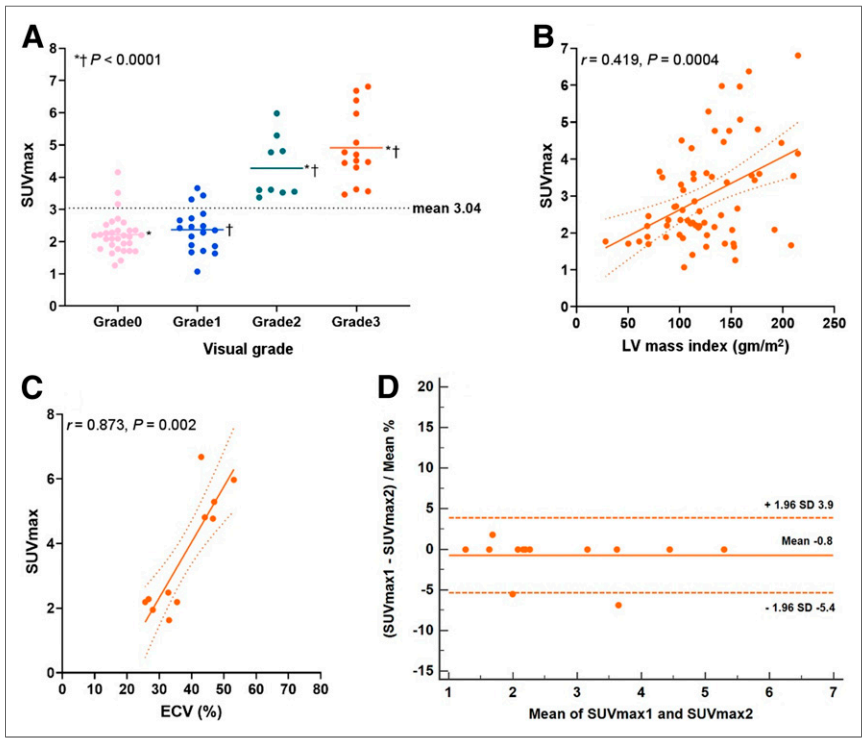

FIGURE 2. ^{99m}Tc-pyrophosphate SUV_{max} distribution by visual grade (A), its correlation to LVMI (B), its correlation to ECV (C), and its repeatability using Bland–Altman plots (D). SUV_{max} was similar in grades 0 and 1 and was similar but higher in grades 2 and 3. Correlation to LVMI (n = 67) was moderate, and correlation to ECV (n = 11) was strong. Bland–Altman plots show excellent repeatability, with coefficient of variation of 1.7%. Dotted line represents mean for entire cohort (A), SE (B and C), or SD (C).

TABLE 2
Quantitative ^{99m}Tc-pyrophosphate Imaging Metrics

Imaging metric	No ATTR CA (n = 49)	ATTR CA (n = 23)	P
SUV_{mean}	1.3 ± 0.3	2.4 ± 0.6	<0.0001
SUV_{max}	2.3 ± 0.6	4.7 ± 1.1	<0.0001
CAA	513 ± 196	1263 ± 461	<0.0001
%ID	0.61 ± 0.23	1.59 ± 0.54	<0.0001

Data are mean ± SD.

The sensitivity of the CZT SPECT system in a standard-sized patient is about 10% higher than that of the NaI(Tl)-based γ-camera (*11*). The CZT camera also offers slightly better resolution than the NaI(Tl) camera. It has been shown that dead-time losses at a high count rate are negligible for the CZT camera for the activity range in clinical exams (*12*). In principle, these results can be extrapolated to other CZT SPECT/CT systems, but that remains to be studied further.

The results of the ROC curve analysis indicate that all 4 quantitative metrics were highly accurate for diagnosis of ATTR CA using visual grade as a reference standard; however, there are limitations to this analysis. Visual grading is based on the same images as are used to derive quantitative metrics; this lack of independence ensures high performance. Furthermore, our data suggest that the quantitative metrics may be superior to the reference standard—visual grading—in diagnostic performance.

In a large multicenter study, Gillmore et al. (*2*) evaluated the diagnostic accuracy of ^{99m}Tc-pyrophosphate/DPD/hydroxymethane-diphosphonate in relation to endomyocardial biopsy and reported that a visual grade of 2 or 3 was highly specific (nearly 100%) for diagnosing ATTR CA in patients with heart failure and typical echocardiographic or CMR features of amyloidosis if a monoclonal process is excluded. However, in other studies, the visual grade was not an independent predictor of prognosis (*13,14*); semiquantitative measures of ^{99m}Tc-pyrophosphate or DPD, including a high heart-to-contralateral ratio (*13*) and a high heart–to–whole-body ratio (*15*), showed independent value in predicting worse survival. Similarly, we expect ^{99m}Tc-pyrophosphate absolute quantitative metrics, including SUV_{max}, SUV_{mean}, CAA, and %ID, to play an important role in risk assessment.

Quantitative ^{99m}Tc-pyrophosphate imaging offers a specific molecular signal of amyloidosis that is likely to play an important role in the detection of early disease and in the assessment of response to novel TTR stabilizing (*16*) or novel TTR silencing therapies. Whether the grade 0 and 1 patients with higher quantitative metrics in this cohort represent early ATTR CA is difficult to ascertain, as this study was based on a referral cohort of patients with heart failure. Screening of a community-based cohort of older individuals for age-related wild-type ATTR CA using ^{99m}Tc-pyrophosphate imaging with longitudinal follow-up, or screening of hereditary ATTR patients for development of hereditary ATTR CA, or performing correlative studies with ECV, would be a better study design to evaluate the value of quantitative metrics in early disease detection.

Our results demonstrate, in a small cohort, a strong correlation between quantitative ^{99m}Tc-pyrophosphate metrics and ECV, a sensitive and quantitative measure of cardiac amyloid burden that has served as a marker of prognosis in amyloid light-chain (*17*) and ATTR (*18*) CA. As in our study, Ross et al. (*9*) demonstrated similarly high correlations between ^{99m}Tc-DPD %ID and ECV in 44 patients. Together, these 2 studies support the value of the %ID of ^{99m}Tc-pyrophosphate and DPD in estimating cardiac amyloid burden; larger studies are warranted.

In this study, we evaluated 4 quantitative metrics: SUV_{max}, representing a single voxel value; SUV_{mean}, representing the mean of all voxels in the LV VOI; CAA, representing the product of SUV_{mean} and LV volume; and %ID, representing the product of mean activity concentration within the LV VOI and its volume, normalized to injected dose. Three of the 4 quantitative metrics showed high repeatability, suggesting that they have utility in evaluating response to therapy. Of the quantitative metrics studied, SUV_{max} is of limited value, as it is determined by a single voxel value in the entire VOI and can be contaminated by spillover from overlapping bone activity. SUV_{mean} is an average over the entire LV (and blood pool) and may better represent the burden of ATTR CA, but this metric may be insensitive to early disease, which may start focally; furthermore, it is very sensitive to VOI definition

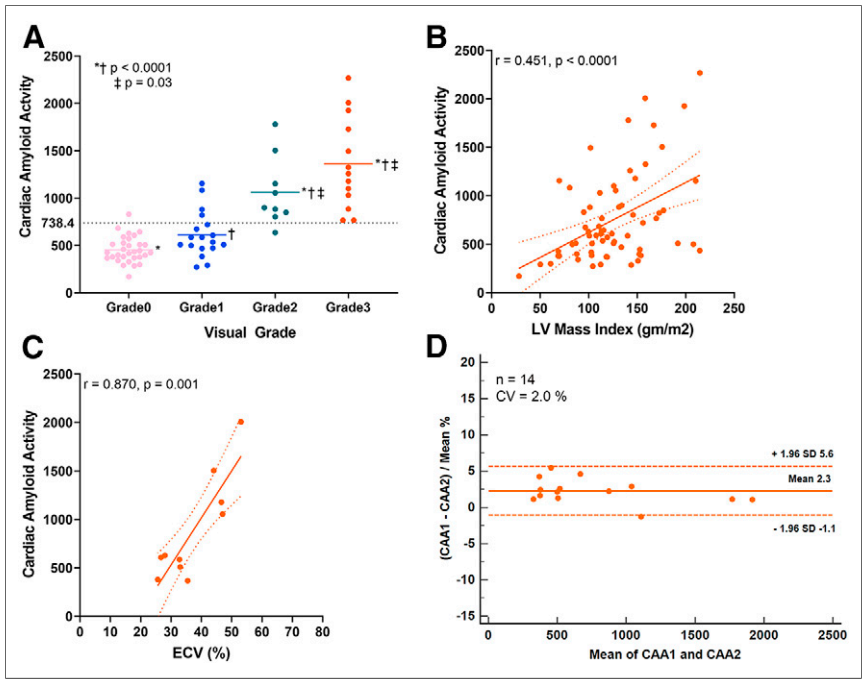

FIGURE 3. ^{99m}Tc-pyrophosphate CAA distribution by visual grade (A), its correlation to LVMI (B), its correlation to ECV (C), and its repeatability using Bland–Altman plots (D). CAA was similar in grades 0 and 1 and was similar but higher in grades 2 and 3. Correlation to LVMI (n = 67) was moderate, and correlation to ECV (n = 11) was strong. Bland–Altman plots show excellent repeatability, with coefficient of variation of 2.0%. In A, 1 mCi = 37 MBq. CAA is reported in g.

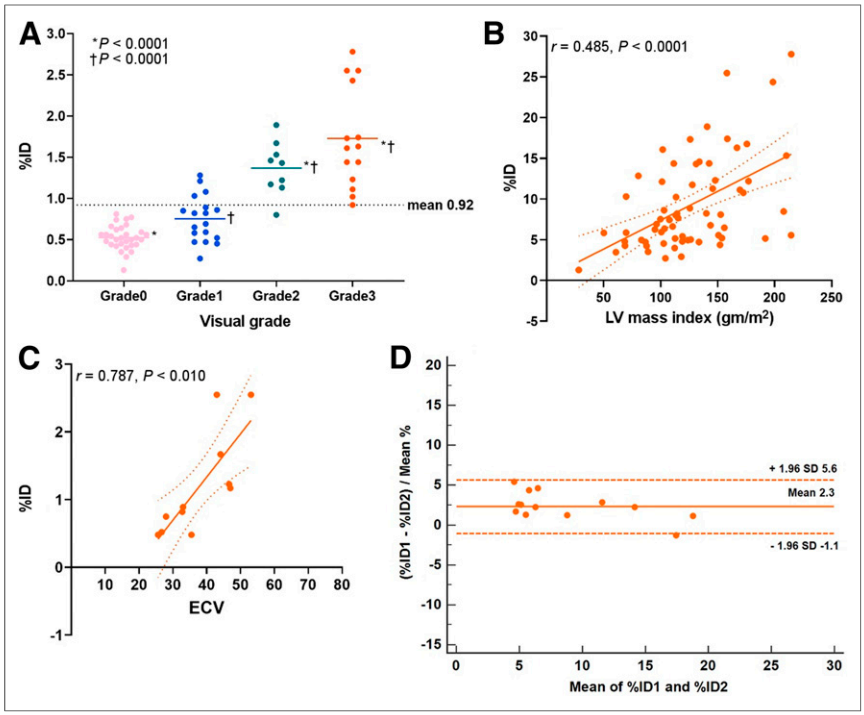

FIGURE 4. ^{99m}Tc-pyrophosphate %ID distribution by visual grade (A), its correlation to LVMI (B), its correlation to ECV (C), and its repeatability using Bland–Altman plots (D). %ID was similar in grades 0 and 1 and was similar but higher in grades 2 and 3. Correlation to LVMI (n = 67) was moderate, and correlation to ECV (n = 11) was strong. Bland–Altman plots show excellent repeatability, with coefficient of variation of 2.0%.

and, therefore, less repeatable than the other metrics. CAA and %ID are volumetric metrics that take into account myocardial volume. Although SUV_{max} and SUV_{mean} performed as well as CAA and %ID in terms of correlation to standard metrics of amyloid burden, CAA and %ID may prove superior to SUV_{max} and SUV_{mean} for risk stratification and assessment of response to therapy. Finally, SUV_{max}, SUV_{mean}, and CAA incorporate normalization to body weight, which is not optimal for highly specific tracers. This issue may be a factor in the apparent superiority of %ID.

This observational study included a small number of patients with ECV, the current reference standard for amyloid burden. Previously studied ^{99m}Tc-pyrophosphate metrics, that is, heart–to–whole-body retention index and heart-to-contralateral ratio, were not evaluated in this study, as early imaging and planar imaging data, respectively, were not available. A high SUV_{max} in patients with visual grade 0 or 1 could represent excess blood-pool activity, but that possibility is less likely because the duration between injection and scan was 150–180 min. Despite these limitations, this study of 72 patients is, to the best of our knowledge, the largest report to date on quantitative ^{99m}Tc-pyrophosphate SPECT/CT (*8*) and the first report on quantitative ^{99m}Tc-pyrophosphate imaging using a 360° CZT SPECT/CT with advanced reconstruction algorithms.

CONCLUSION

Absolute quantitative metrics derived from ^{99m}Tc-pyrophosphate SPECT/CT images are moderately to strongly correlated with traditional structural markers of cardiac amyloid burden, and furthermore, SUV_{max}, CAA, and %ID are highly repeatable. CAA and %ID are promising tomographic quantitative metrics of cardiac amyloid burden; future studies validating their role for detection of early disease, assessment of response to therapy, and stratification of risk are warranted.

DISCLOSURE

Sharmila Dorbala has received consulting fees from Pfizer and GE Healthcare; an investigator-initiated grant from Pfizer; and research support from the U.S. National Institutes of Health/National Heart, Lung, and Blood Institute (grants R01 HL130563 and HL150342) and the American Heart Association (grant AHA 16 CSA 28880004) for amyloidosis. Sarah Cuddy has received an investigator-initiated research grant from Pfizer. Rodney Falk has received consulting fees from Ionis Pharmaceuticals, Alnylam Pharmaceuticals, and Caelum Biosciences; research funding from GlaxoSmithKline and Akcea; and research support from the U.S. National Institutes of Health/National Heart, Lung, and Blood Institute (grant R01 HL130563). Marcelo Di Carli has received a research grant from Spectrum Dynamics and Gilead and consulting fees from Sanofi and GE. No other potential conflict of interest relevant to this article was reported.

ACKNOWLEDGMENTS

We thank Christopher Breault for his help with image export and image analysis training.

TABLE 3
Linear Regression Analyses

Model	Dependent variable	Independent variable	R^2	Standardized coefficient	t	P
1	LVMI	SUV_{max}	0.175	0.419 (95% CI, 0.193–0.645)	3.716	<0.001
2	LVMI	SUV_{mean}	0.105	0.324 (95% CI, 0.090–0.558)	2.761	0.007
3	LVMI	CAA	0.194	0.440 (95% CI, 0.218–0.662)	3.953	<0.001
4	LVMI	%ID	0.235	0.485 (95% CI, 0.269–0.701)	4.474	<0.001

KEY POINTS

QUESTION: Can myocardial amyloid burden be quantified by ^{99m}Tc-pyrophosphate imaging using advanced CZT SPECT/CT scanner technology with a 360° detector configuration?

PERTINENT FINDINGS: In 72 persons with known or suspected CA undergoing quantitative ^{99m}Tc-pyrophosphate CZT SPECT/CT imaging, we found that absolute quantitative metrics derived from ^{99m}Tc-pyrophosphate images are moderately to strongly correlated with traditional structural markers of cardiac amyloid burden on echocardiography (n = 67) or CMR (n = 11) and highly repeatable.

IMPLICATIONS FOR PATIENT CARE: Quantitative ^{99m}Tc-pyrophosphate SPECT/CT offers the potential for early detection, risk stratification, and monitoring of response to therapy in patients with CA.

REFERENCES

1. Dorbala S, Ando Y, Bokhari S, et al. ASNC/AHA/ASE/EANM/HFSA/ISA/SCMR/SNMMI expert consensus recommendations for multimodality imaging in CA: part 1 of 2—evidence base and standardized methods of imaging. *J Nucl Cardiol.* 2019;26:2065–2123.
2. Gillmore JD, Maurer MS, Falk RH, et al. Nonbiopsy diagnosis of cardiac transthyretin amyloidosis. *Circulation.* 2016;133:2404–2412.
3. Hutton BF, Erlandsson K, Thielemans K. Advances in clinical molecular imaging instrumentation. *Clin Transl Imaging.* 2018;6:31–45.
4. Dibble EH, Alvarez AC, Truong MT, Mercier G, Cook EF, Subramaniam RM. ^{18}F-FDG metabolic tumor volume and total glycolytic activity of oral cavity and oropharyngeal squamous cell cancer: adding value to clinical staging. *J Nucl Med.* 2012;53:709–715.
5. Mitchell C, Rahko PS, Blauwet LA, et al. Guidelines for performing a comprehensive transthoracic echocardiographic examination in adults: recommendations from the American Society of Echocardiography. *J Am Soc Echocardiogr.* 2019;32:1–64.
6. Cuddy SAM, Bravo PE, Falk RH, et al. Improved quantification of cardiac amyloid burden in systemic light chain amyloidosis: redefining early disease? *JACC Cardiovasc Imaging.* 2020;13:1325–1336.
7. Fujita N, Duerinekx AJ, Higgins CB. Variation in left ventricular regional wall stress with cine magnetic resonance imaging: normal subjects versus dilated cardiomyopathy. *Am Heart J.* 1993;125:1337–1345.
8. Caobelli F, Braun M, Haaf P, Wild D, Zellweger MJ. Quantitative ^{99m}Tc-DPD SPECT/CT in patients with suspected ATTR CA: feasibility and correlation with visual scores. *J Nucl Cardiol.* 2020;27:1456–1463.
9. Ross JC, Hutt DF, Burniston M, et al. Quantitation of ^{99m}Tc-DPD uptake in patients with transthyretin-related CA. *Amyloid.* 2018;25:203–210.
10. Bailey DL, Willowson KP. An evidence-based review of quantitative SPECT imaging and potential clinical applications. *J Nucl Med.* 2013;54:83–89.
11. Desmonts C, Bouthiba MA, Enilorac B, Nganoa C, Agostini D, Aide N. Evaluation of a new multipurpose whole-body CzT-based camera: comparison with a dual-head Anger camera and first clinical images. *EJNMMI Phys.* 2020;7:18.
12. Erlandsson K, Kacperski K, van Gramberg D, Hutton BF. Performance evaluation of D-SPECT: a novel SPECT system for nuclear cardiology. *Phys Med Biol.* 2009;54:2635–2649.
13. Castano A, Haq M, Narotsky DL, et al. Multicenter study of planar technetium 99m pyrophosphate cardiac imaging: predicting survival for patients with ATTR CA. *JAMA Cardiol.* 2016;1:880–889.
14. Hutt DF, Fontana M, Burniston M, et al. Prognostic utility of the Perugini grading of ^{99m}Tc-DPD scintigraphy in transthyretin (ATTR) amyloidosis and its relationship with skeletal muscle and soft tissue amyloid. *Eur Heart J Cardiovasc Imaging.* 2017;18:1344–1350.
15. Rapezzi C, Quarta CC, Guidalotti PL, et al. Role of ^{99m}Tc-DPD scintigraphy in diagnosis and prognosis of hereditary transthyretin-related CA. *JACC Cardiovasc Imaging.* 2011;4:659–670.
16. Maurer MS, Schwartz JH, Gundapaneni B, et al. Tafamidis treatment for patients with transthyretin amyloid cardiomyopathy. *N Engl J Med.* 2018;379:1007–1016.
17. Banypersad SM, Fontana M, Maestrini V, et al. T1 mapping and survival in systemic light-chain amyloidosis. *Eur Heart J.* 2015;36:244–251.
18. Martinez-Naharro A, Kotecha T, Norrington K, et al. Native T1 and extracellular volume in transthyretin amyloidosis. *JACC Cardiovasc Imaging.* 2019;12:810–819.